The CGILS experimental design to investigate low cloud feedbacks in general circulation models by using single-column and large-eddy simulation models

Minghua Zhang, Christopher S. Bretherton, Peter N. Blossey, Sandrine Bony, Florent Brient, J.-C Golaz

The CGILS experimental design to investigate low cloud feedbacks in general circulation models by using single-column and large-eddy simulation models

Minghua Zhang,[1] Christopher S. Bretherton,[2] Peter N. Blossey,[2] Sandrine Bony,[3] Florent Brient,[3] and Jean-Christophe Golaz[4]

Received 31 July 2012; revised 20 September 2012; accepted 26 October 2012; published 22 December 2012.

[1] A surrogate climate change is designed to investigate low cloud feedbacks in the northeastern Pacific by using Single Column Models (SCMs), Cloud Resolving Models (CRMs), and Large Eddy Simulation models (LES), as part of the CGILS study (CFMIP-GASS Intercomparison of LES and SCM models). The constructed large-scale forcing fields, including subsidence and advective tendencies, and their perturbations in the warmer climate are shown to compare well with conditions in General Circulation Models (GCMs), but they are free from the impact of any GCM parameterizations. The forcing fields in the control climate are also shown to resemble the mean conditions in the ECMWF-Interim Reanalysis. Applications of the forcing fields in SCMs are presented. It is shown that the idealized design can offer considerable insight into the mechanisms of cloud feedbacks in the models. Caveats and advantages of the design are also discussed.

Citation: Zhang, M., C. S. Bretherton, P. N. Blossey, S. Bony, F. Brient, and J.-C. Golaz (2012), The CGILS experimental design to investigate low cloud feedbacks in general circulation models by using single-column and large-eddy simulation models, *J. Adv. Model. Earth Syst., 4,* M12001, doi:10.1029/2012MS000182.

1. Introduction

[2] Cloud-climate feedback has been a dominant source of model discrepancies in projections of future climate change [e.g., *Randall et al.*, 2007; *Andrews et al.*, 2012]. Understanding and narrowing these discrepancies requires better knowledge of the mechanisms of cloud feedbacks in the models. Because clouds interact with the large-scale atmospheric dynamics through radiation and latent heating, and because their simulation often relies on several types of physical parameterizations in the General Circulation Models (GCMs), such an understanding is still very limited, especially in terms of intermodel differences [*Bony et al.*, 2006].

[3] The objective of this paper is to present the design of an idealized experimental framework used to investigate the mechanism of cloud feedback with Single-Column Models (SCMs), Cloud-Resolving Models (CRM), and Large Eddy Simulation models (LES), for the CFMIP-GASS Intercomparison of LES and SCM models (CGILS). The challenge of the design is to obtain large-scale forcing fields that are representative of climate changes in GCMs, but are independent of them; these forcing fields should be close to observations, but they should be applicable to climate changes. Idealized experimental designs have been used in other areas of model development. These include *Held and Suarez* [1994] and *Jablonowski and Williamson* [2006] for dynamical cores of GCMs, aqua-planet experiments [*Neale and Hoskins*, 2000; *Medeiros et al.*, 2008], and cloud process case studies in GCSS (GEWEX Cloud System Studies) [e.g., *Siebesma et al.,* 2004; *Stevens et al.*, 2005].

[4] The present study builds on the work of *Zhang and Bretherton* [2008]. We target the response of clouds to a climate change of uniformly raised sea-surface temperature (SST) by 2°C (referred to as the Cess Experiment [*Cess et al.*, 1990]), along the Pacific Cross-Section Intercomparison (GPCI) region in the north tropical to subtropical Pacific [*Teixeira et al.*, 2011]. In GCMs, cloud feedbacks from the Cess experiments have been shown to capture intermodel differences of feedbacks in the equilibrium response of slab ocean models to doubling of CO_2 [*Ringer et al.*, 2006]. The GPCI is chosen as the study region because it covers the transition of stratocumulus to shallow cumulus and then to deep convection. Figures 1a and 1b show the amount of low clouds and total cloud amount in the summer from

[1]School of Marine and Atmospheric Sciences, State University of New York at Stony Brook, Stony Brook, New York, USA.
[2]Department of Atmospheric Sciences, University of Washington, Seattle, Washington, USA.
[3]Laboratoire de Meteorologie Dynamique, Institute Pierre Simon Laplace, Paris, France.
[4]Geophysical Fluid Dynamics Laboratory, NOAA, Princeton, New Jersey, USA.

1942-2466/12/2012MS000182

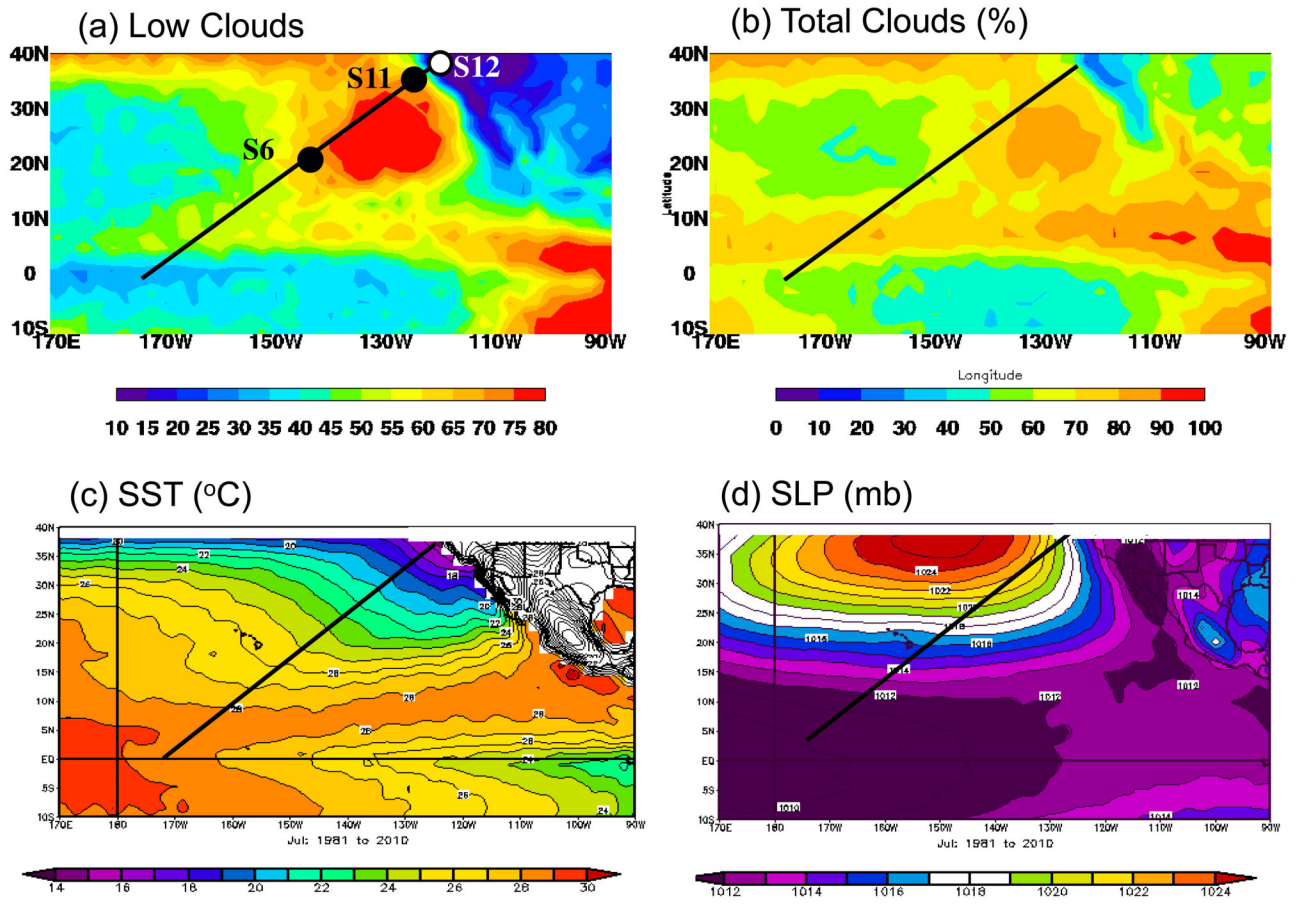

Figure 1. (a) Averaged amount of low clouds in June-July-August (%), and (b) total cloud amount from the C3M satellite data. Note the different color scales. The black line is the GPCI (see text); the symbols "S6", "S11" and "S12" are the three locations used in the paper. (c and d) The corresponding sea surface temperature (SST) and sea level pressure (SLP).

the composite of the A-train integrated CALIPSO, CloudSat, CERES, and MODIS merged satellite product (C3M) averaged in June-July-August from 2006 to 2009 [*Sato et al.*, 2011]. The clouds in the northeast Pacific correspond to some of the strongest net cloud radiative forcing in the world. Their variations in climate change simulations have been reported as important to cloud feedbacks in GCMs [*Bony and Dufresne* 2005; *Webb et al.*, 2006; *Zelinka et al.*, 2012].

[5] In addition to designing the large-scale forcing fields in a changed climate, this paper also discusses the changes of the large-scale environment in the GCM Cess experiments and compares them with the idealized forcing. These changes, in particular the intermodel differences, are important to understand the response of clouds in this region and the discrepancies among the models.

[6] The paper is organized as follows. Section 2 briefly describes the data and GCM simulations. Section 3 introduces the construction of the control climate, laying the foundation for that of the perturbed climate. Section 4 gives the large-scale forcing in the perturbed climate and comparison with GCM results. Section 5 shows two examples of using the idealized design to gain physical insights about cloud feedbacks. The last section contains a brief summary and discussion.

2. Data and Models

[7] The atmospheric data used in this study are from the ECMWF Interim Reanalysis (Interim-ERA) [*Dee et al.,* 2011] for July 2003, which was among the first few months available to us and is representative of climatological July conditions. Simulation results from three GCMs were taken from those conducted by the Climate Process Team (CPT) on Low Cloud Feedbacks. These are the Community Atmospheric Model (CAM) Version 3.1 (CAM3) [*Collins et al.,* 2006], the Geophysical Fluid Dynamics Laboratory (GFDL) Atmospheric Model Version 2 (AM2) [*GMAT*, 2004], and the CAM3 with super-parameterizations in which cloud resolving models (CRM) are embedded in each grid box of the GCM (SPCAM) [*Khairoutdinov and Randall*, 2001]. Cloud feedbacks in these three models from the Cess experiments have been reported in *Wyant et al.* [2006], *Medeiros et al.* [2008] and *Wyant et al.* [2009]. We primarily use the CAM3 and AM2 in the discussions of the GCM environment. The SPCAM is included only

when appropriate, since CAM3 and AM2 better represent operational climate models. Newer versions of these models are now available [*Donner et al.*, 2011; R. B. Neale et al., The mean climate of the Community Atmosphere Model (CAM4) in forced SST and fully coupled experiments, submitted to *Journal of Climate*, 2012], but we do not expect their inclusion to affect the results of this study.

[8] The terminology used in the paper is as follows: CTL denote control climate; P2S denotes the warmer or perturbed climate in which SST is uniformly raised by 2°C (subsidence is also changed, hence the letter "S"). Horizontal advective tendencies of temperature and water vapor are also referred to as advections for simplicity. We use the term "CGILS fields" to refer to the variables in the idealized design.

3. Characteristics of Large-Scale Forcing in the Control Climate

3.1. State Variables

[9] Figures 1c and 1d show the sea-surface temperature (SST) and sea-level pressure (SLP) distributions in the northern summer. Figure 2 shows the atmospheric temperature, relative humidity, and winds along the GPCI in the Interim-ERA, which are used as the CGILS control climate. The surface air temperature decreases from the equator to the coast by about 10°C near the surface (Figure 2a) as in the SST. Above the altitude of the 800 hPa level, the weak-temperature gradient approximation holds true in the summer [*Sobel et al.,* 2001]. The relative humidity (RH; Figure 2b) is less than 30% in the bulk of the free troposphere north of 15°N; the RH minimum is below 10% at 20°N and 500 hPa.

[10] The low level winds (Figures 2c and 2d) are northerly near the coast, easterly at the equator, and northeasterly in between, consistent with the surface pressure field in Figure 1d. At the upper levels, the northern portion of the cross section is located to the east of the middle-Pacific trough that is sandwiched between the two continental high pressure centers over South Asia and North America, hence the winds are southwesterly, but the southern portion of the cross section is in the equatorial easterly. The wind distributions in Figures 2c and 2d resemble the Walker circulation but it is along the GPCI.

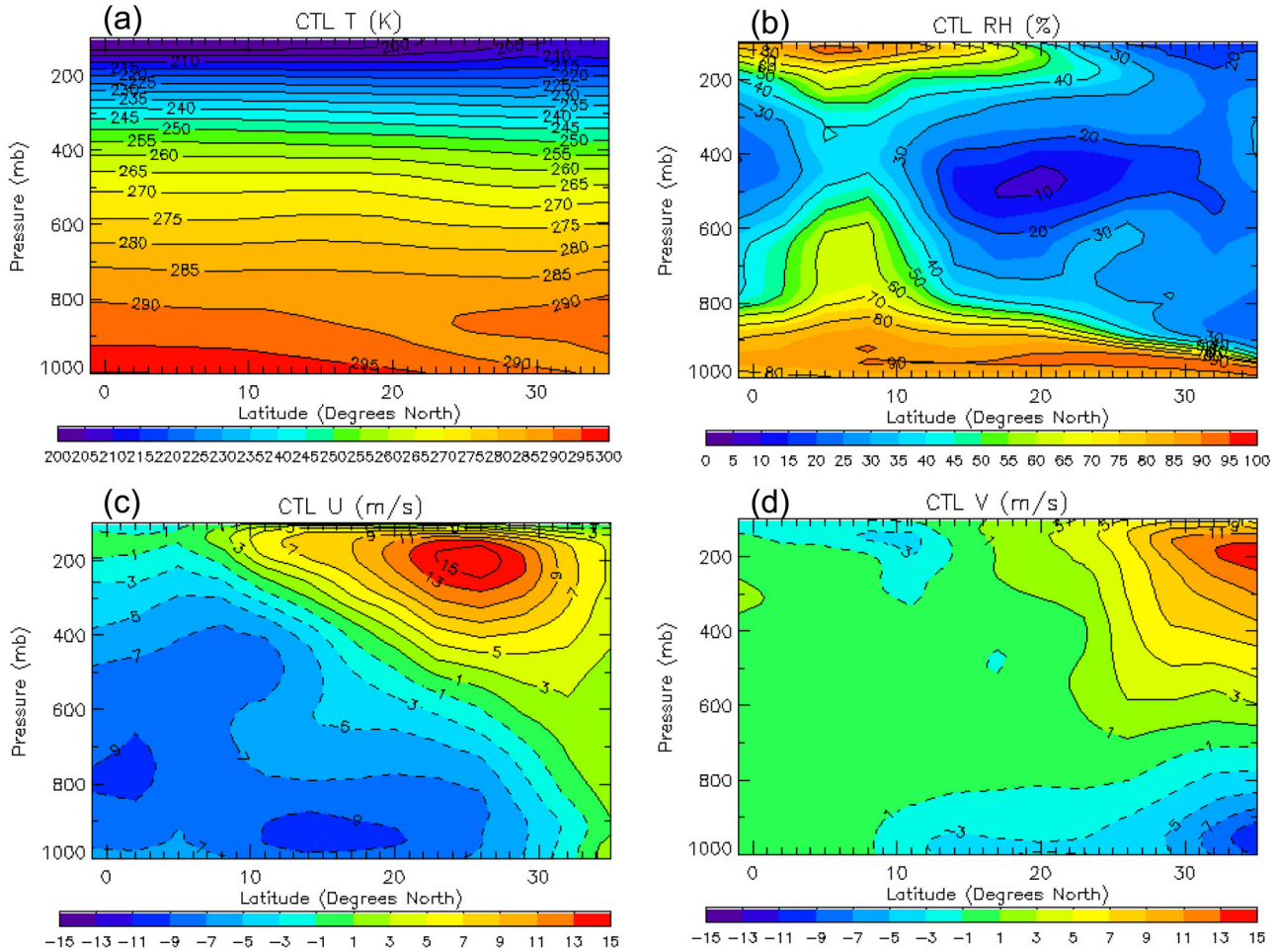

Figure 2. Atmospheric state variables along the GPCI for July 2003 from Interim-ERA, which are used in the control climate. (a) temperature, (b) relative humidity, (c) eastward component U of winds, (d) northward component V of winds.

[11] The large-scale vertical pressure velocity is derived rather than taken from Interim-ERA, because the modification of the Interim-ERA vertical velocity in the perturbed climate is less straightforward than for temperature. This idealized vertical pressure velocity is based on the steady-state energy balance of the free troposphere

$$\left(\vec{V}\cdot\nabla\theta\right)_{LS}+\omega\frac{\partial\theta}{\partial p}=Q_R \tag{1}$$

where Q_R is the net clear-sky radiative cooling. Other terms are as commonly used. Q_R is calculated by using the state variables, with a solar constant of 1367 W/m^2, surface albedo of 0.07 and July 15 insolation, and the RRTM radiation code [*Mlawer et al.*, 1997] as implemented in CAM5. Ozone was obtained from interpolation by using the standard atmosphere profiles in the tropics (equator) and middle latitude summer (45°N). The vertical shape of the subsidence rate ω is specified as follows:

$$\omega(p)=$$

$$\begin{cases} A\times\cos\left[(p_m-p)/(p_m-100)\times\dfrac{\pi}{2}\right],\ for\ 100mb<p\le p_m \\ A\times\cos\left[(p-p_m)/(p_s-p_m)\times\dfrac{\pi}{2}\right],\ for\ p_m<p\le p_s \end{cases}$$

where p_m is equal to 750 mb and p_s is the surface pressure. The amplitude A of ω is calculated by using the vertically integrated Interim-ERA horizontal tendencies from 900 hPa to 300 hPa (p_1 to p_2):

$$\int_{p_1}^{p_2}\omega\frac{\partial\theta}{\partial p}dp=\int_{p_1}^{p_2}Q_R dp-\int_{p_1}^{p_2}\left(\vec{V}\cdot\nabla\theta\right)_{LS}dp$$

[12] Imposing the shape of the vertical profile of ω is equivalent to assuming the spatial pattern of the large-scale atmospheric circulation (wind divergences). It simplifies the derivation of the perturbed climate and the interpretation of the model results. The above procedure is used only for the coastal location of S12 shown in Figure 1a. At other locations, the amplitude A is scaled by the Interim-ERA ratio of ω at these locations to that of S12 at 750 hPa. The ω fields from this idealization and Interim-ERA are shown in Figures 3a and 3b. Also shown in Figure 3 are the corresponding distributions in the CAM3 (Figure 3c) and in AM2 (Figure 3d). Overall, the CTL ω field of CGILS captures the essential features in the Interim-ERA and GCMs and is within their range.

3.2. Advective Tendencies

[13] Within the boundary layer, the horizontal advective tendencies along the GPCI tend to cool and dry the boundary layer, as the winds carry boundary layer air from cooler SSTs to warmer SSTs along the cross-section. In the CGILS framework, the advection of temperature from the surface to 900 hPa is calculated from

$$\begin{aligned}-\left(\vec{V}\cdot\nabla\theta\right)_S &= -\left|\vec{V}_s\right|\cdot|\nabla T_s|\cos\left(\vec{V}_s,\nabla T_s\right)\\ &= -\left|\vec{V}_s\right|\frac{\partial SST}{\partial l}\frac{\cos\left(\vec{V}_s,\nabla T_s\right)}{\cos\left(\vec{l},\nabla T_s\right)}\end{aligned} \tag{2}$$

where the last term, containing the angles of the cross section (l) with the SST gradient and surface winds, is derived from fitting (2) to the Interim-ERA monthly mean value. The horizontal advection of the water vapor is calculated from

$$-\left(\vec{V}\cdot\nabla q\right)_S=-\left(\vec{V}\cdot\nabla T\right)_S\left(RH_s\frac{\partial q_s}{\partial T}\right) \tag{3}$$

where RH_s is the surface relative humidity.

[14] The horizontal advective tendencies of temperature and water vapor in the free troposphere are obtained as residuals from the steady-state clear-sky equations

$$-\left(\vec{V}\cdot\nabla\theta\right)_{LS}=\omega\frac{\partial\theta}{\partial p}-Q_R \tag{4}$$

$$-\left(\vec{V}\cdot\nabla q\right)_{LS}=\omega\frac{\partial q}{\partial p} \tag{5}$$

which are applied above 800 hPa. Between 800 and 900 hPa, the advective tendencies are linearly interpolated by using values at 900 hPa and at 800 hPa for each latitude.

[15] Figure 4a shows the derived horizontal advective tendency of temperature for CGILS. There is cold advection along the GPCI in the lower troposphere that is consistent with the northeastly winds; there is also cold advection in the middle troposphere near the coast, which is associated with westerly winds at these altitudes to advect cool air from the ocean to land. These features are similar to Interim-ERA in Figure 4b and to CAM3 and AM2 (Figures 4c and 4d). Note that in Interim-ERA and to a lesser extent in the GCMs, the impact of the PBL is obvious in the northern GPCI, with a maximum of positive advection right above the boundary layer due to the slope of the PBL height. In our design, this impact is intentionally removed, because imposing a large warming advection above and cooling advection below tends to lock the PBL height at that level. Indeed, when SCMs and LESs are forced with large-scale forcing from the GCMs or Interim-ERA, they tend to simulate clouds that behave like those in the select GCM or in Interim-ERA. This indicates the need of idealized design that is independent of GCM physical parameterizations for SCM and LES intercomparison studies.

[16] Figure 5a shows the derived horizontal advection of water vapor mixing ratio in CGILS. Besides the

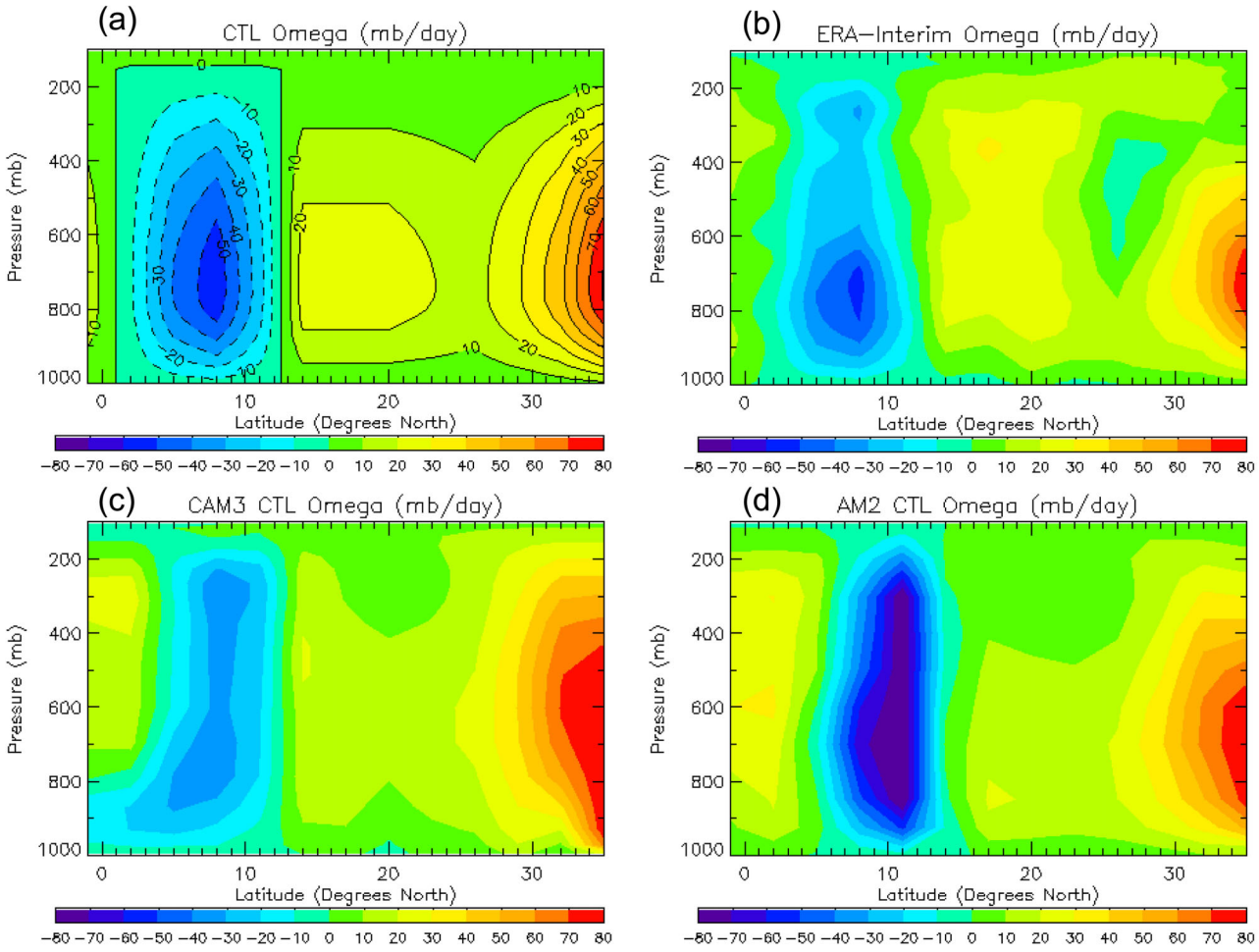

Figure 3. Pressure vertical velocity in the idealized control climate (a), and comparison with Interim-ERA (b), CAM3 (c), and AM2 (d).

atmospheric state variables, the only other input in its derivation is the vertical velocity and surface temperature advection. This can be compared with Interim-ERA, CAM3 and AM2 in Figures 5b–5d. The patterns are similar in all products; the CGILS magnitude is also similar to Interim-ERA. In the Interim-ERA, however, there is a distinct signature of drying right at the PBL top that corresponds to the warming in Figure 4b. Note the large dry advection in the two GCMs near the surface relative to Interim-ERA, especially in CAM3. This is caused by the known biases of overestimated strength of the subtropical high and excessive near-surface wind speeds in the models. The impact of these biases on the model clouds is not clear.

4. Change of Large-Scale Forcing in a Warmer Climate

[17] In the perturbed climate, SST is uniformly raised by 2°C along the GPCI. Several large-scale fields are assumed fixed. These include the horizontal winds, relative humidity, and the vertically integrated horizontal temperature advection at S12. The perturbed fields include the temperature, water vapor mixing ratio, large-scale vertical motion, and advective tendencies of temperature and humidity. The temperature perturbation at the ITCZ latitude (10°N) is based on an undiluted air parcel rising adiabatically to the tropopause with surface air relative humidity at 80%. The weak-temperature gradient approximation is then used for all other latitudes. In the stratosphere, the increase ramps linearly from the tropopause to zero at 50 hPa. Figure 6a gives the temperature perturbation. Corresponding to the 2°C surface warming, the atmosphere warms about 5°C at 300 hPa. This can be compared with those in the SPCAM, CAM, and AM2 in Figures 6b–6d. The CGILS perturbation is within the range of the model results.

[18] The large-scale subsidence at S12 is perturbed accordingly using the procedure for the control climate, due to the changes in the static stability and radiative cooling in equation (1). The radiative cooling change is caused by the changes in SST, air temperature, and water vapor. At other latitudes, the change is imposed by using the same scaling factors from Interim-ERA. In Figure 7, we show the profiles of the pressure vertical velocity at three locations along the GPCI, which are labeled as S6, S11 and S12 in Figure 1a, representing the

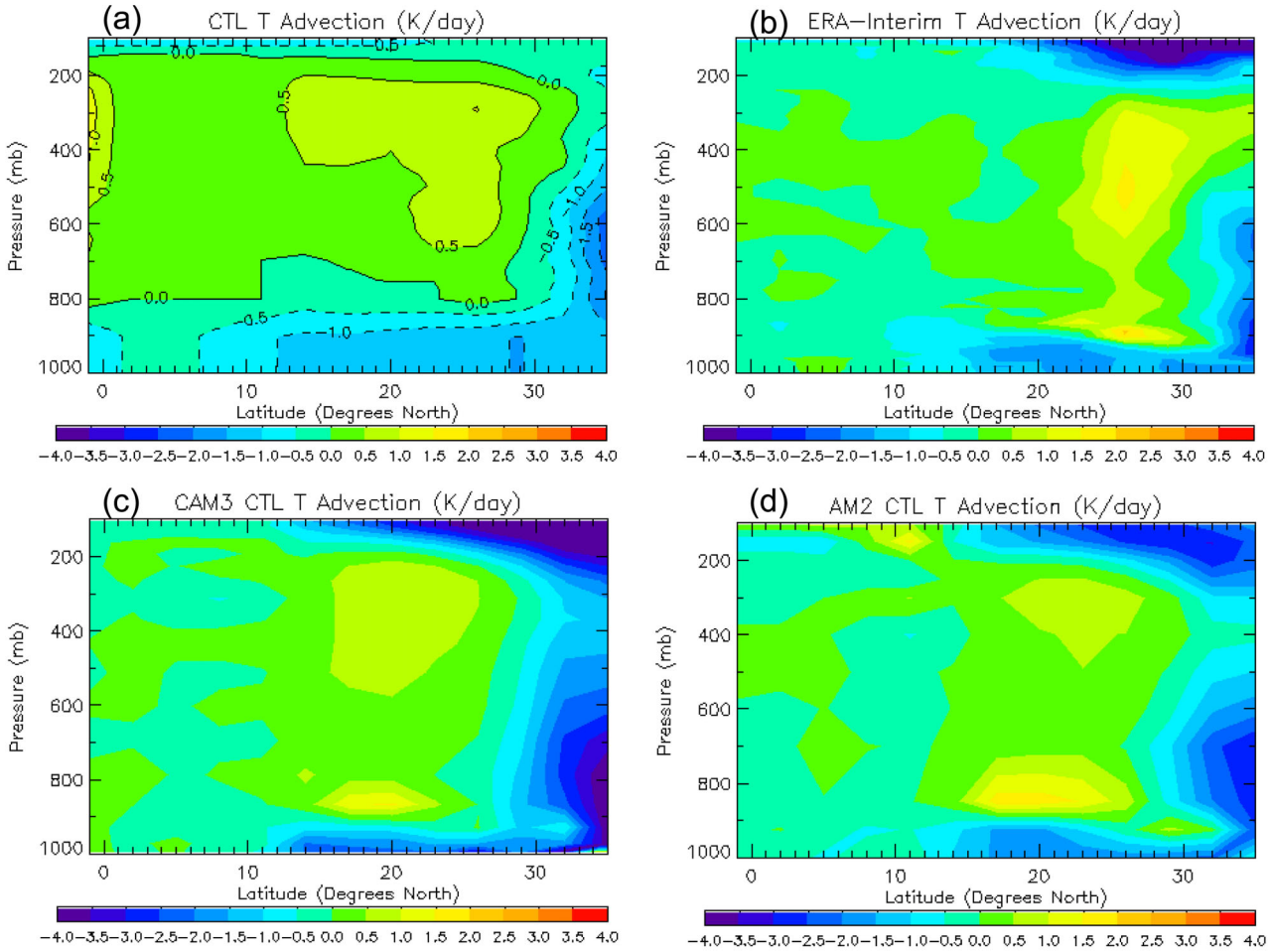

Figure 4. Same as Figure 3 except for horizontal advective tendency of temperature.

cloud regimes of shallow cumulus, cumulus under stratocumulus, and coastal stratocumulus respectively. The black solid line is for the CGILS CTL; black dashed line is for CGILS P2S. The red solid line is for Interim-ERA. Also shown are comparisons of CTL and P2S in CAM3 (orange) and AM2 (green). The positions and surface meteorological variables of the three locations are listed in Table 1. Because at S12 the CGILS P2S subsidence is weaker than the CTL subsidence, its vertical motion at all other latitudes is also weaker in P2S. This is also true in all models, but there are substantial intermodel differences as shown in the Figure 7. The CGILS reduction is constrained by the change in static stability and radiative cooling, with the former dominating. These constraints also apply to the models, but there horizontal advection of temperature also changes differently in the different GCMs.

[19] Figure 8 shows the corresponding comparison of the horizontal temperature advection. The advective cooling in the two models, especially the CAM3, is considerably larger than the Interim-ERA, which is also plotted. This explains why the model CTL subsidence in Figure 7 is stronger than in CGILS. The intermodel differences are substantial, but they should become smaller if averaged over a large domain. These differences may not be as significant as they appear for SCM and LES applications, since there is cancellation between the vertical and horizontal advections, and equation (1) is still the fundamental constraint on the three-dimensional forcing of temperature.

[20] The corresponding P2S and CTL comparison of the horizontal humidity advective tendency is given in Figure 9. The CGILS near-surface drying is stronger in P2S than in CTL at all locations. This is due to the temperature dependence of surface specific humidity in equation (3). Notice that at S12, in the GCMs, especially the CAM3, there is very large moist advection in the lower troposphere away from the surface. This corresponds to the larger subsidence drying in the models than in Interim-ERA and in CGILS.

[21] We wish to also comment on the validity of the fixed winds and relative humidity assumed for CGILS P2S. As shown in several studies [e.g., *Zhang and Song*, 2006; *Vecchi et al.,* 2006; M. J. Webb and A. Lock, Coupling between subtropical cloud feedback and the local hydrological cycle in a climate model, submitted to *Climate Dynamics*, 2012], GCM winds are weaker in a warmer climate. These can be seen in Figure 10 for CAM3 and AM2 relative to their mean winds that have similar patterns to the Interim-ERA mean winds in Figures 2c

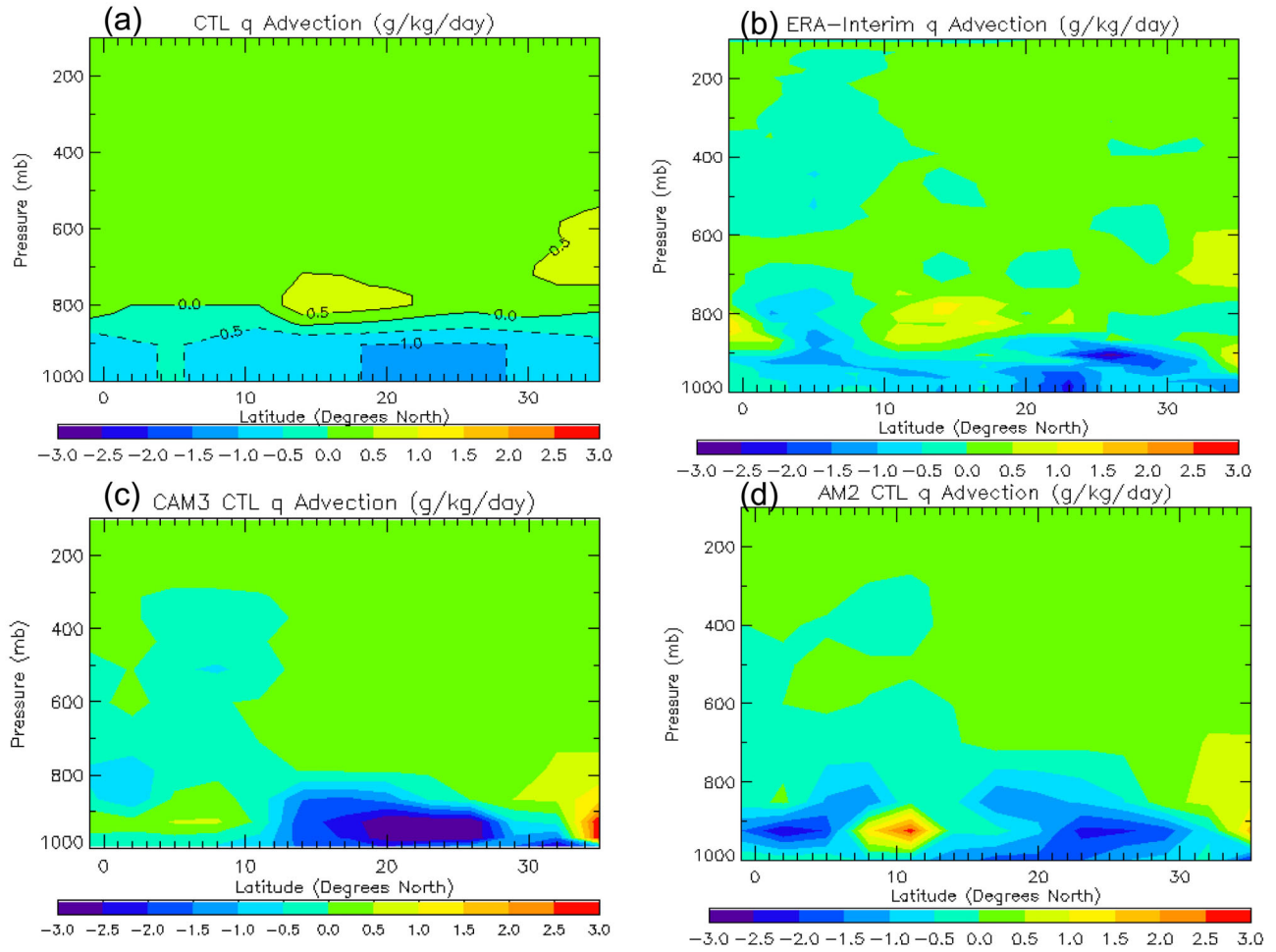

Figure 5. Same as Figure 3 except for horizontal advective tendency of water vapor mixing ratio.

and 2d. The implication to CGILS is the impact of the wind change on the forcing fields and on the surface fluxes. The effect on the horizontal advective tendencies should have been incorporated in the derived subsidence based equations (4) and (5), so this should not be an issue. The maximum changes of winds appear to be in the upper troposphere; the surface change is less than 1 m/s, but its effect on the surface flux and near-surface advection is not clear. Since the GCMs differ greatly in this respect, we did not include this effect in the CGILS design. For the relative humidity, in the two GCMs, the P2S values are higher than the CTL by an average of 2% near 800 hPa, but lower by 4% near 400 hPa (not shown). Since the free tropospheric humidity effectively serves as an upper boundary condition on simulations of boundary layer clouds, changes in free tropospheric relative humidity may impact cloud feedbacks (C. S. Bretherton et al., A large-eddy simulation of mechanisms of boundary layer cloud response to climate change in CGILS, submitted to the *Journal of Advances in Modeling Earth Systems*, 2012). But because the patterns and magnitudes of the relative humidity change are very different in the models, and there is no simple theory to design the change, we did not include it in CGILS.

[22] With the above information, we have all the forcing fields for both CTL and P2S to carry out SCM or LES integrations. These fields represent the GCM environment and yet they are independent of model parameterizations; these fields resemble Interim-ERA in the control climate, but they can also describe a warmer climate. This is exactly the objective of the CGILS idealized design. The features of the large-scale forcing fields described above in the GCM are also relevant to understand clouds in the models.

[23] It should be pointed out that in the derived CGILS fields, only the free troposphere obeys the controlling equations of (4)–(5). Below 900 hPa, the advective cooling and drying are to be balanced by surface fluxes, precipitation, latent heating, cloud radiative effects, and the interactive vertical advection terms in SCMs and LESs [*Randall and Cripe*, 1999]. It is the interaction of these processes that produces clouds, and CGILS intends to describe this environment to represent GCM conditions.

[24] We also note that although the focus of CGILS is on low clouds, the forcing fields are derived along the whole GPCI, including the deep tropics. In regions of large-scale ascent, the scaling of vertical motion by the clear-sky subsidence can probably be justified. In all three GCMs, the upward motion between 5°N to 10°N is weaker in the P2S climate (not shown), even though

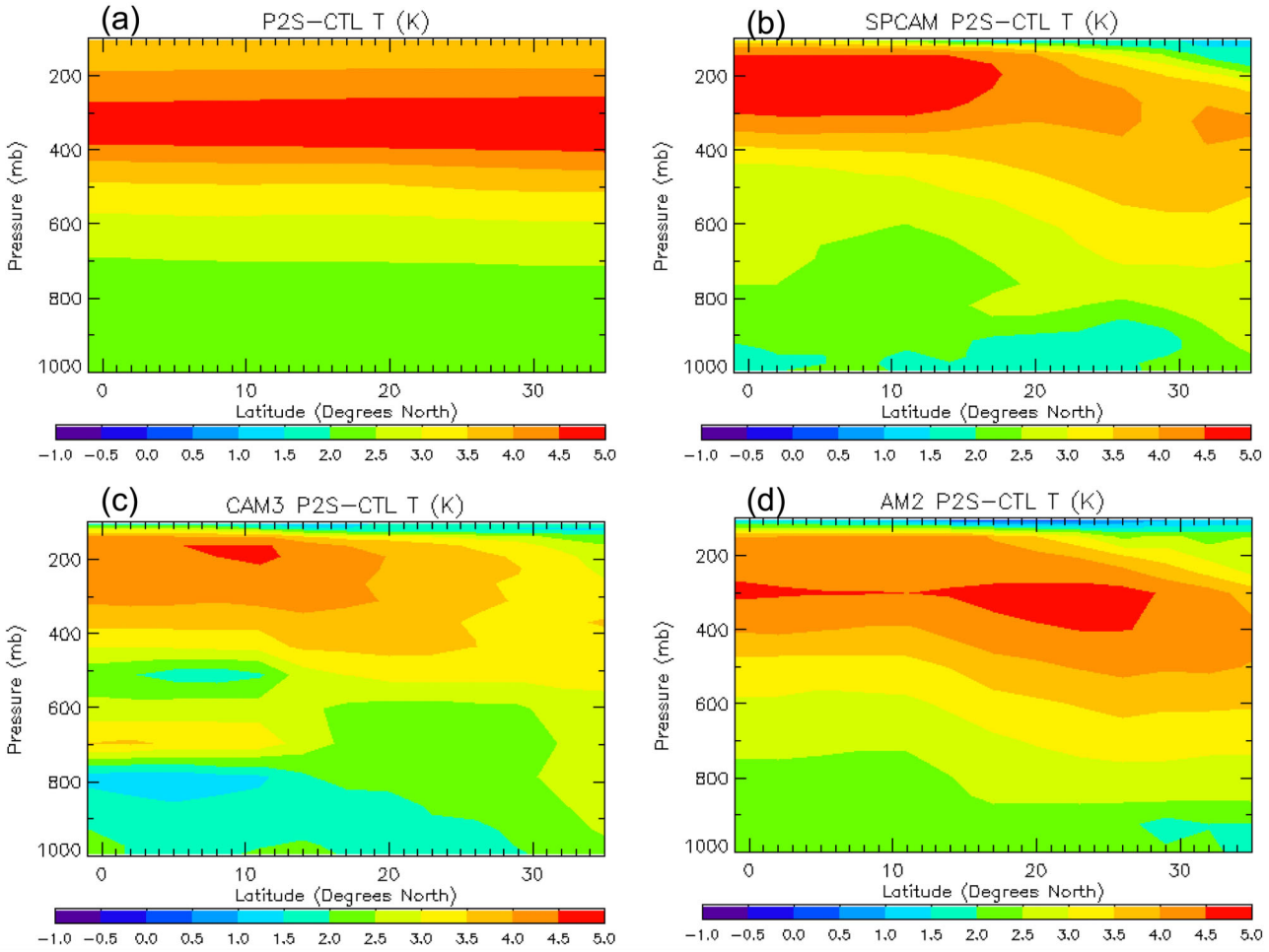

Figure 6. Temperature change from control (CTL) to warmer (P2S) climate in: (a) CGILS, (b) SPCAM, (c) CAM3, and (d) AM2.

the magnitudes of the reductions differ by a factor of two among the models. The horizontal advective tendencies based on clear-sky calculation in the ascending portion of the GPCI are more problematic. But because the horizontal temperature advection in the deep tropics is small, the derived tendency from (4) does not differ much from the Interim-ERA and GCM values. For water vapor, we set horizontal advective tendency to

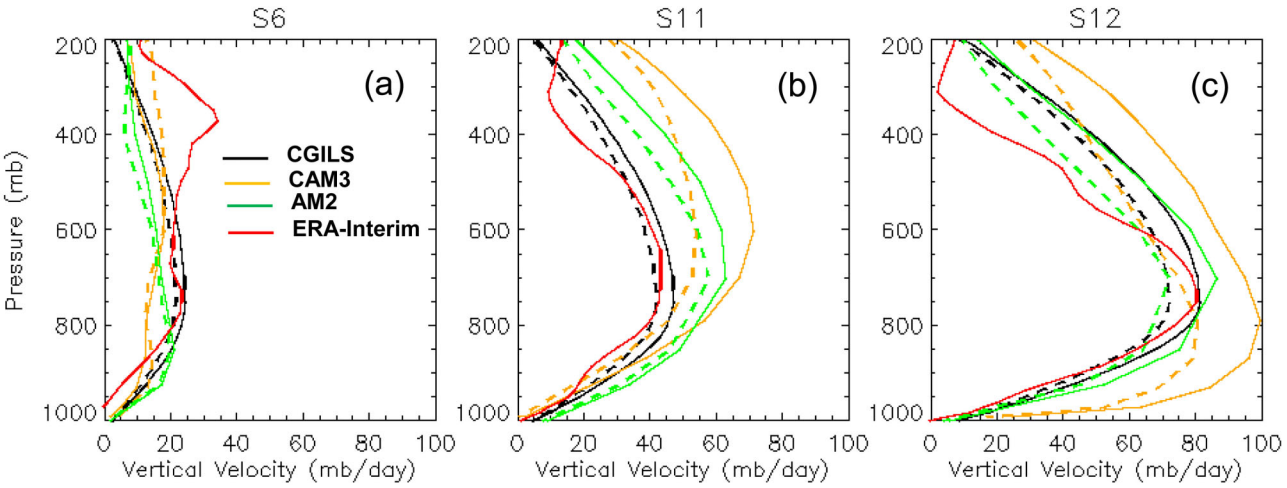

Figure 7. Pressure vertical velocity in CTL (solid lines) and P2S (dashed lines) climates in CGILS, CAM3 and AM2 at locations (a) S6, (b) S11, and (c) S12.

Table 1. Location and Surface Meteorological Conditions at the Three Locations

	S6 Shallow Cu	S11 Stratocumulus	S12 Stratus
Latitude (Degrees North)	17°N	32°N	35°N
Longitude (Degrees)	149°W	129°W	125°W
SLP (mb)	1014.1	1020.8	1018.6
SST (°C)	25.6	19.3	17.8
Tair_surface (°C)	24.1	17.8	16.3
U_surface (m/s)	−7.4	−1.8	2.1
V_surface (m/s)	−2.7	−6.5	−8.0
RH_surface (m/s)	80%	80%	80%
Mean TOA insolation (w/m2)	448.1	471.5	473.1
Mean daytime solar zenith angle	51.0	52.0	52.7
Daytime fraction on July 15	0.539	0.580	0.590
Eccentricity on July 15	0.967	0.967	0.967
Surface Albedo	0.07	0.07	0.07

zero when the motion is upward. This excluded the dry intrusions from middle latitudes, but the change of the horizontal water vapor advection from CTL to P2S is much smaller than that of the vertical advection, so this simplification may be acceptable.

5. Applications

[25] We present two applications of the CGILS forcing data in this section, to illustrate both the values of the experimental design and caveats in their use. The caveats address the limitations of the forcing data in representing the spatial pattern and transient behavior of the GCM environment.

5.1. Simulated Clouds and Their Climate Change Responses in CAM3

[26] We first show results using the CAM3 SCM. A similar idealized setup to CGILS was used in *Zhang and Bretherton* [2008] who analyzed the cause of the negative cloud feedback in the model. The CGILS setup differs from their study in that horizontal advective tendencies are included, and that the locations span the whole GPCI rather than just one location.

[27] Figures 11a and 11c compare the cloud distributions of the CTL climate along the GPCI, in the GCM and in its SCM with CGILS forcing. Despite the constant and idealized forcing, the simulated clouds by the SCM is remarkably similar to that in the GCM, except for the cirrus clouds near the tropopause level, which is not expected because there is no transport of water vapor in the SCM away from convection detrainment across the grids. The low-cloud layers also occur higher in the SCM than in the GCM. Nevertheless, the overall similarity affords considerably simplified analysis of the physical parameterization, and the possibility of comparison with CRM or LES simulations.

[28] The corresponding simulations for the P2S clouds are in Figure 11b for GCM and in Figure 11d for SCM in CGILS. An important cloud response of the CAM3 GCM to SST warming is the increase of low clouds, leading to its negative cloud feedback [e.g., *Wyant et al.*, 2006]. This is seen along the GPCI. The increase of low clouds from CTL to P2S is also captured in the SCM as in Figure 11d relative to Figure 11c. This similarity allows more in-depth study of the cloud feedback processes as in *Zhang and Bretherton* [2008].

[29] As a caveat, SCM cloud responses along the GPCI may not be the same as those in the GCMs for all models. This is not just because of the idealized setup,

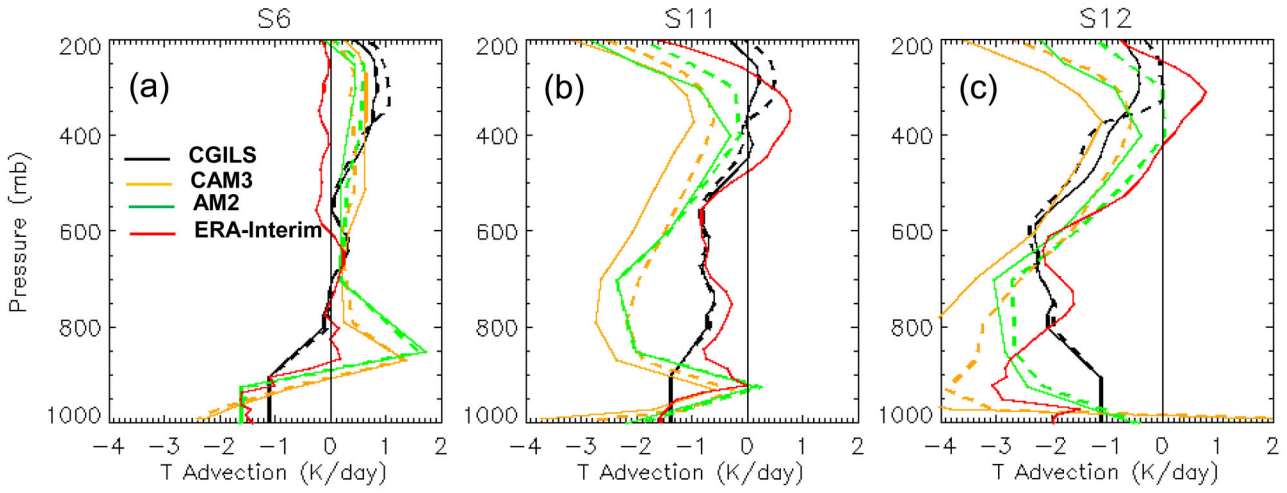

Figure 8. Same as Figure 7 except for horizontal advective tendency of temperature.

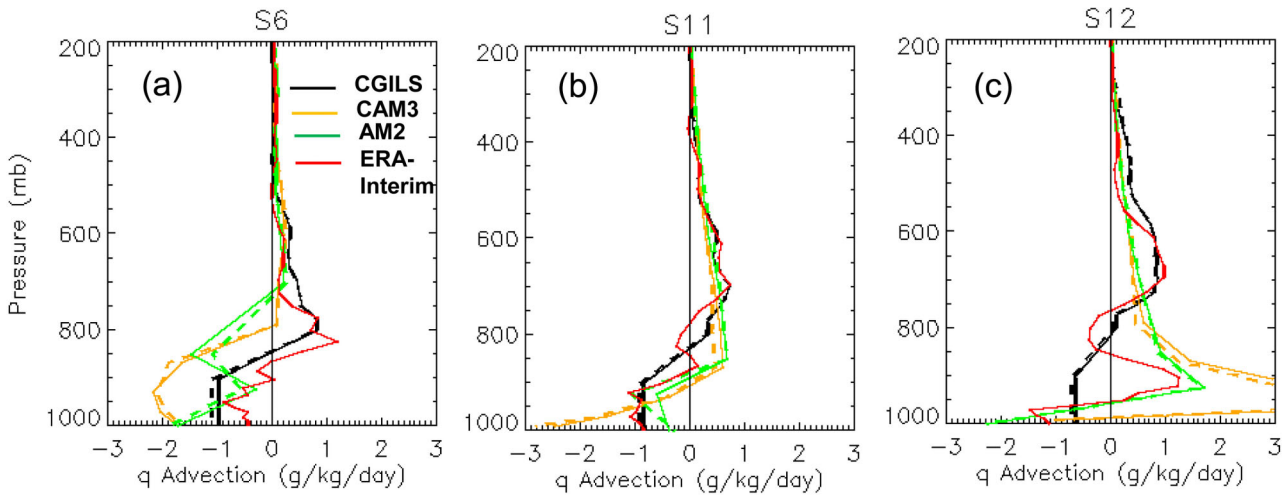

Figure 9. Same as Figure 7 except for horizontal advective tendency of water vapor mixing ratio.

but also because of the spatial sampling of the GPCI in representing the GCM behavior in the subtropical eastern Pacific. In fact, the cloud response to warming can be spatially noisy due to the impact of synoptic variations. Figure 12a shows the distribution change of CAM3 cloud radiative forcing (CRF) from CTL to P2S. Although there is an overall negative change of CRF (negative feedback) in the tropics from 30°N to 30°S, a randomly

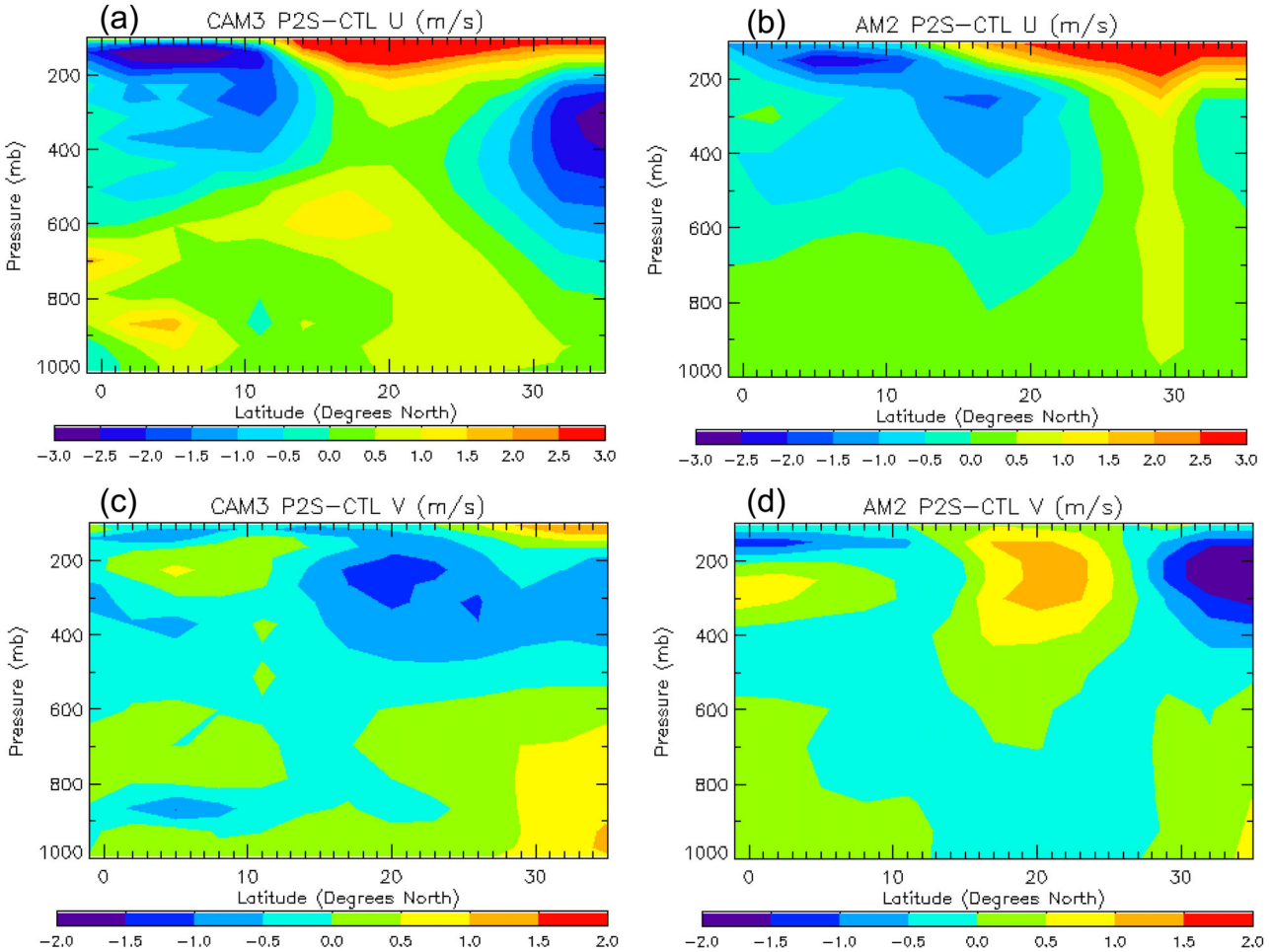

Figure 10. Difference of wind components between P2S and CTL along the GPCI. (a and c) For the U, V components for CAM3; (b and d) for AM2.

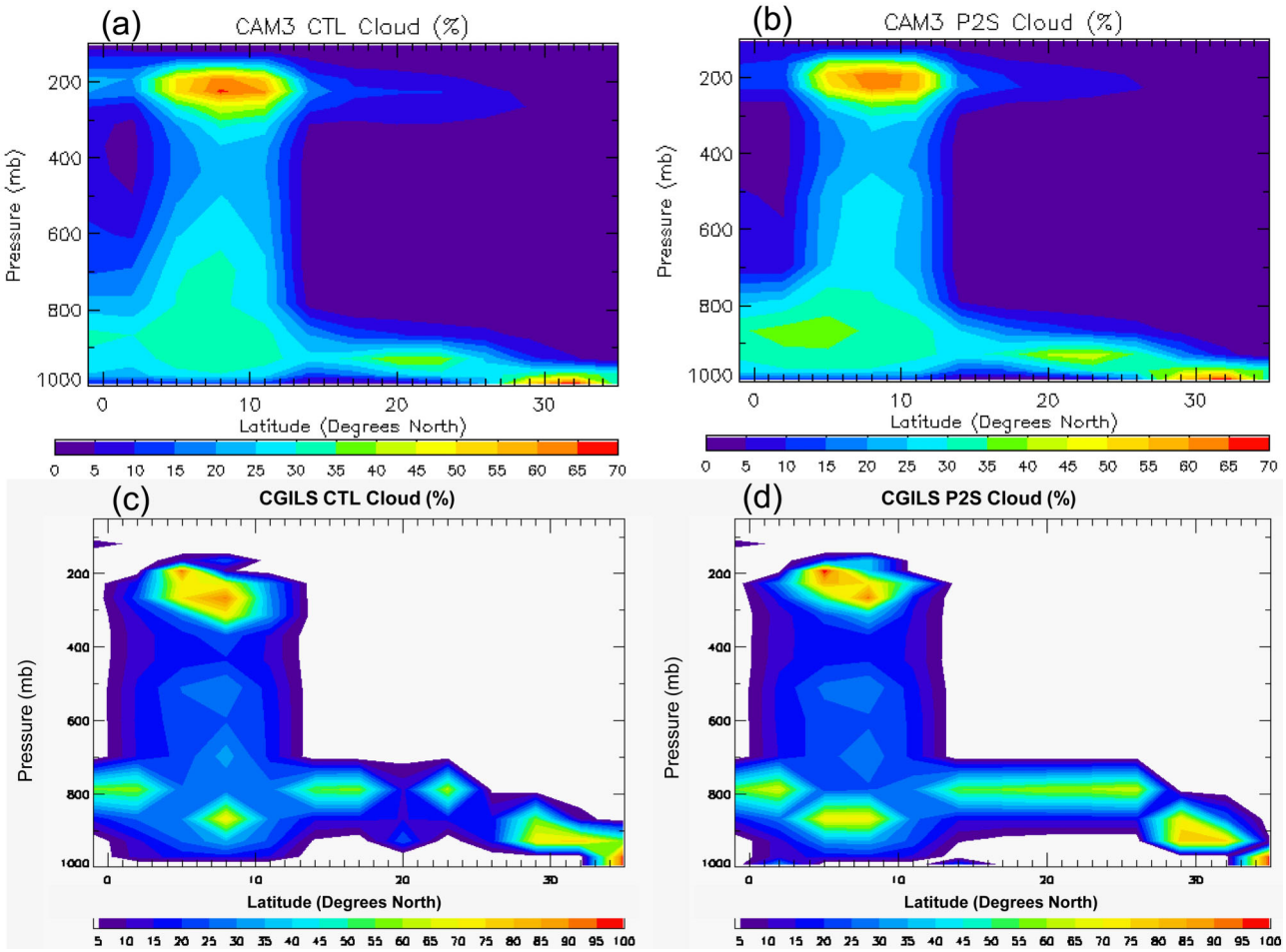

Figure 11. (a and b) Cloud amount simulated in the CTL and P2S experiments respectively by the CAM3 GCM. (c and d) CGILS simulations using SCMs.

chosen cross section may not represent the sign of the change for the whole tropics. In the case of CAM3, the GPCI happens to sample the main change. Figure 12b shows the CRF change in the SPCAM. In this case, the cross section well represents the study region, and so comparison with CGILS along the GPCI can be more direct. Therefore, it is recommended that SCM results are better compared with the GCM along the GPCI if the GCM has a coherent spatial pattern; otherwise they should be compared with the GCM by appropriately sampling statistics of cloud responses. The CGILS setup in fact has the advantage of minimizing the spatial noise due to the lack of synoptic variability, which can be model dependent.

5.2. Impact of Transient Forcing

[30] Aside from the spatial sampling discussed above, there is no guarantee that the LES and SCM results by using steady-state forcing can fully capture processes with transient forcing, because clouds respond to external forcing nonlinearly. The steady forcing may cause grid locking of clouds in SCMs that misses intended processes.

[31] We discuss how results from the steady forcing can be still useful to gain insights about the models. We added two types of transience to the rate of subsidence in the forcing. One type is stochastically generated by using the temporal variances of vertical velocity from the Institute Pierre Simon Laplace (IPSL) model [*Hourdin et al.,* 2006], with no consideration of its time scale. The second is from the monthly hourly anomalies of vertical velocity in four July months of 2003–2006. *Brient and Bony* [2012] reported both GCM results and SCM results using these forcing fields and the CGILS steady forcing. While the magnitude of the cloud feedback from the steady forcing differs from using the transient forcing, the feedback sign are the same in all cases and with the GCM, which was a positive feedback. To further appreciate their results, we show in Figure 13 the temporal variation of total cloud liquid path at S6 in the CTL (blue line) and P2S (red line) using the IPSL model under steady forcing. Cloud water path is reduced in the warmer climate in the steady forcing case (Figure 13a), leading to a positive cloud feedback. It fluctuates greatly in the two transient cases (Figures 13b and 13c), responding to changes of external forcing, but the five-day moving averages in the CTL and P2S are clearly different, and the difference has the same sign as the steady forcing case. It is also noticed that the time variations in the CTL and P2S are similar under the two

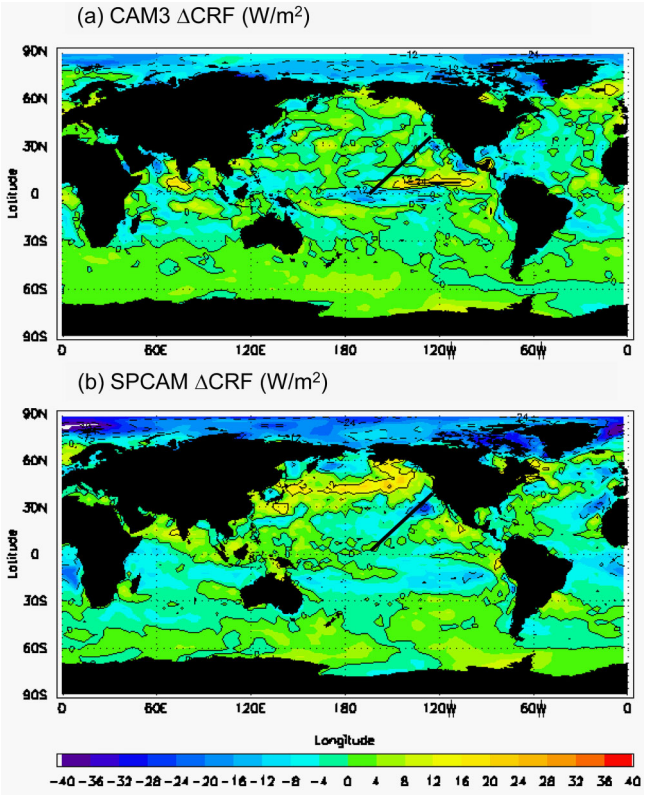

Figure 12. Change of net cloud radiative forcing (CRF) at the top of the atmosphere from CTL to P2S in (a) CAM3, and in (b) SPCAM. The black lines mark the GPCI cross section.

transient cases, especially in Figure 13c. But the perturbation climate adds a difference to the background, which is a reduction of cloud water path in the warmer climate, thus a positive cloud feedback.

[32] The steady forcing however does not always produce results consistent with the transient forcing. Nevertheless, it can still shed important lights to understand the models. We use the GFDL AM3 SCM [*Donner et al.,* 2011] at S11 to demonstrate this. With steady forcing, the model simulated a deeper boundary layer (PBL) and thicker cloud layer at S11 in the warmer climate (Figure 14a, solid blue line for CTL, red dashed line for P2S), thus a negative cloud feedback. Figure 14c shows the water vapor tendencies in the steady forcing CGILS simulations from the parameterizations of PBL, stratiform net evaporation, and shallow convection. It is seen that convection is not active in this case. The negative cloud feedback was found to be caused by the model's stronger turbulent moistening by the PBL scheme in the warmer climate (M. Zhang et al., CGILS: First results from an international project to understand the mechanisms of low cloud feedbacks in general circulation models, submitted to the *Bulletin of the American Meteorological Society*, 2012).

[33] However, when the transient forcing (Interim-ERA variability of subsidence) is used, shallow convection is activated during times of weak subsidence or upward motion, as seen in Figure 14d in the moisture tendency terms. Shallow convection is more active in the warmer climate (Zhang et al., submitted manuscript, 2012), and it dries the cloud layer to reduce the cloud liquid water as seen in Figure 14b, leading to a positive cloud feedback. The enhancement of shallow convection and its impact on the cloud water can be more clearly seen in Figure 15, which shows the convective tendencies of water vapor in the bottom row, and the cloud liquid water in the top row, for the CTL simulations in the left column and P2S in the right column. Again, the climate perturbation adds a background change to the temporal variation of simulated clouds, which is a reduction of cloud water in the warmer climate.

[34] Therefore, the contrast between results from the steady forcing and those from the transient forcing points to the roles of the different parameterization schemes on the cloud feedback. Cloud feedback results from the CGILS SCM simulation should not be expected to necessarily capture those in the parent GCMs. Instead, the CGILS design should be used as a framework to understand the models. As far as SCMs

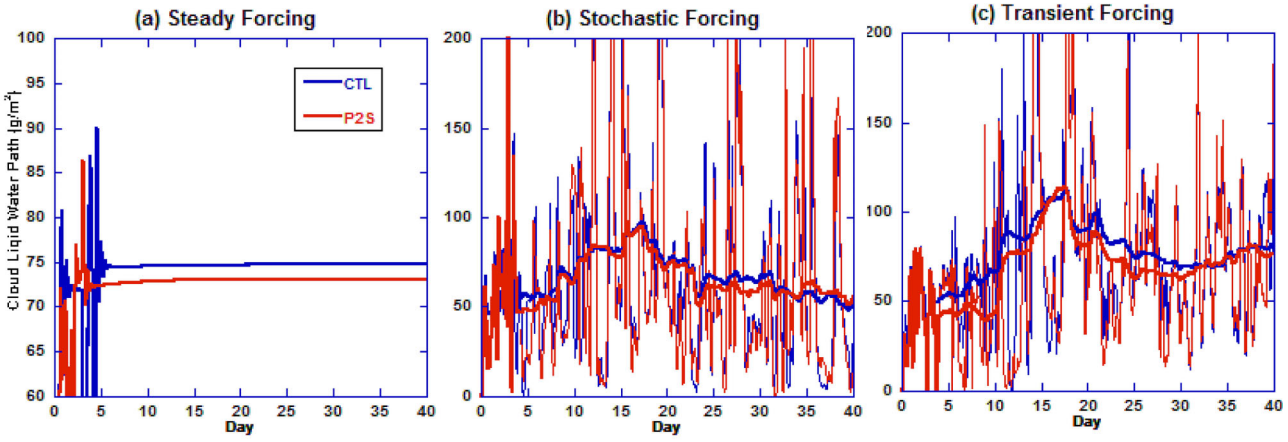

Figure 13. Time series of simulated column cloud liquid water path at S6 for CTL (blue color) and P2S (red color) in the IPSL model under (a) steady-state forcing, (b) stochastic forcing, and (c) transient forcing from Interim-ERA. The thick lines are the five-day running means.

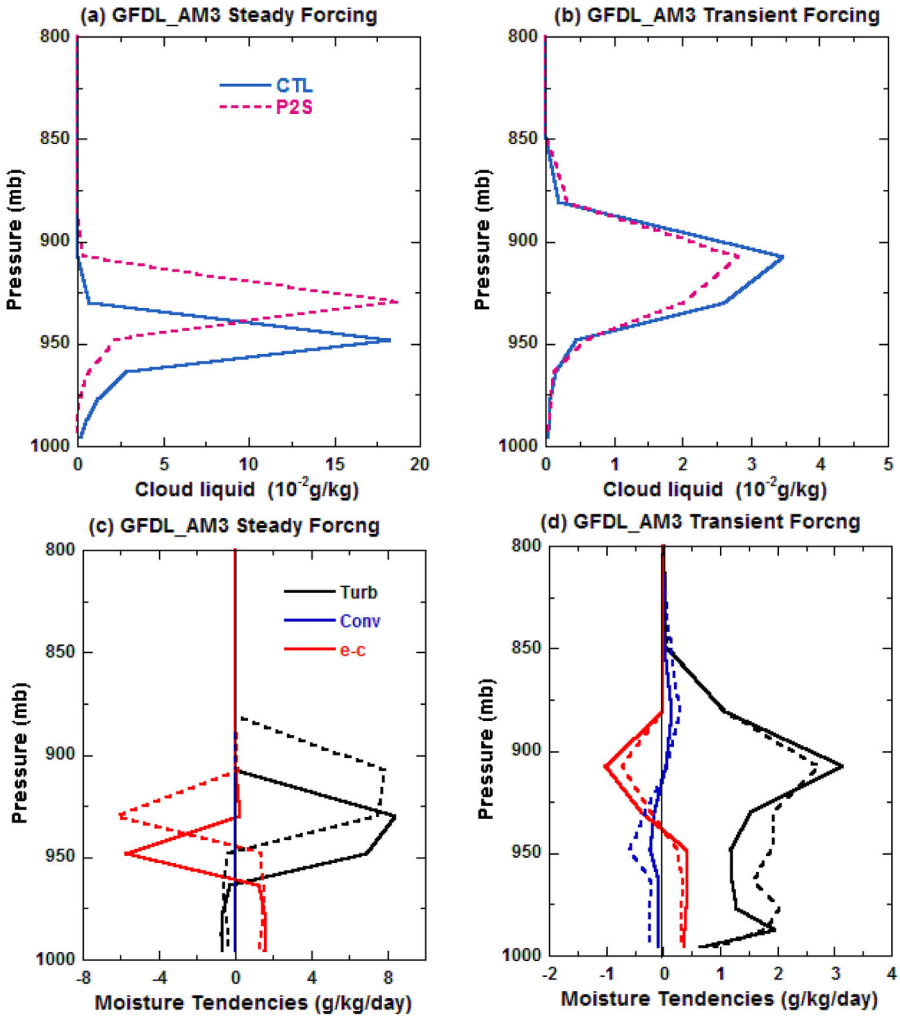

Figure 14. Cloud liquid water in the control (CTL, black solid line) and warmer (P2S, red dashed line) climates in the GFDL model at S11 under (a) steady-state forcing, (b) transient forcing. Physical tendencies of water vapor, "turb" for turbulence scheme, "conv" for convection scheme, "e-c" for net large-scale evaporation, under (c) steady-state forcing, (d) transient forcing.

are concerned, including some temporal variability in the forcing can help to free a model from possibly locked states and better reproduce the cloud behavior simulated in a three-dimensional model, as shown by *Brient and Bony* [2012] for both current and future climate conditions. Therefore, as a supplement to the steady-state forcing fields, CGILS also provides transient forcing products, all at the CGILS website (http://atmgcm.msrc.sunysb.edu/cfmip_figs/Case_specification.html).

6. Summary and Discussion

[35] We have described an experiment design to investigate the response of cloud feedbacks by using SCM and LES models in the Northeast Pacific. Assuming a surrogate climate change of 2°C in SST, the proposed design calculates the large-scale subsidence and horizontal advective tendencies. We have shown that the derived idealized fields capture the essential elements of the GCM environment, yet they are free of the impact of model parameterizations. The fields in the control climate are also similar to the Interim-ERA. The data have been made available to the community. An international comparison project has been carried out using the forcing data from this design, the results of which are described in Zhang et al. (submitted manuscript, 2012) and N. P. Blossey et al. (Interpreting low cloud feedbacks in six large eddy simulation models in the CGILS surrogate climate change, submitted to *Journal of Advances in Modeling Earth Systems*, 2012). The forcing data have been also used by individual modeling groups to understand their GCMs [e.g., *Brient and Bony*, 2012; H. Kawai, Examples of mechanisms for negative cloud feedback of stratocumulus and stratus in cloud parameterizations, submitted to *SOLA*, 2012], and to investigate physical mechanisms in LESs [*Xu et al.,* 2010; Bretherton et al., submitted manuscript, 2012].

[36] We also showed two examples of applying the forcing to understand the mechanisms of cloud feedbacks in models. In one example, the SCM with CGILS

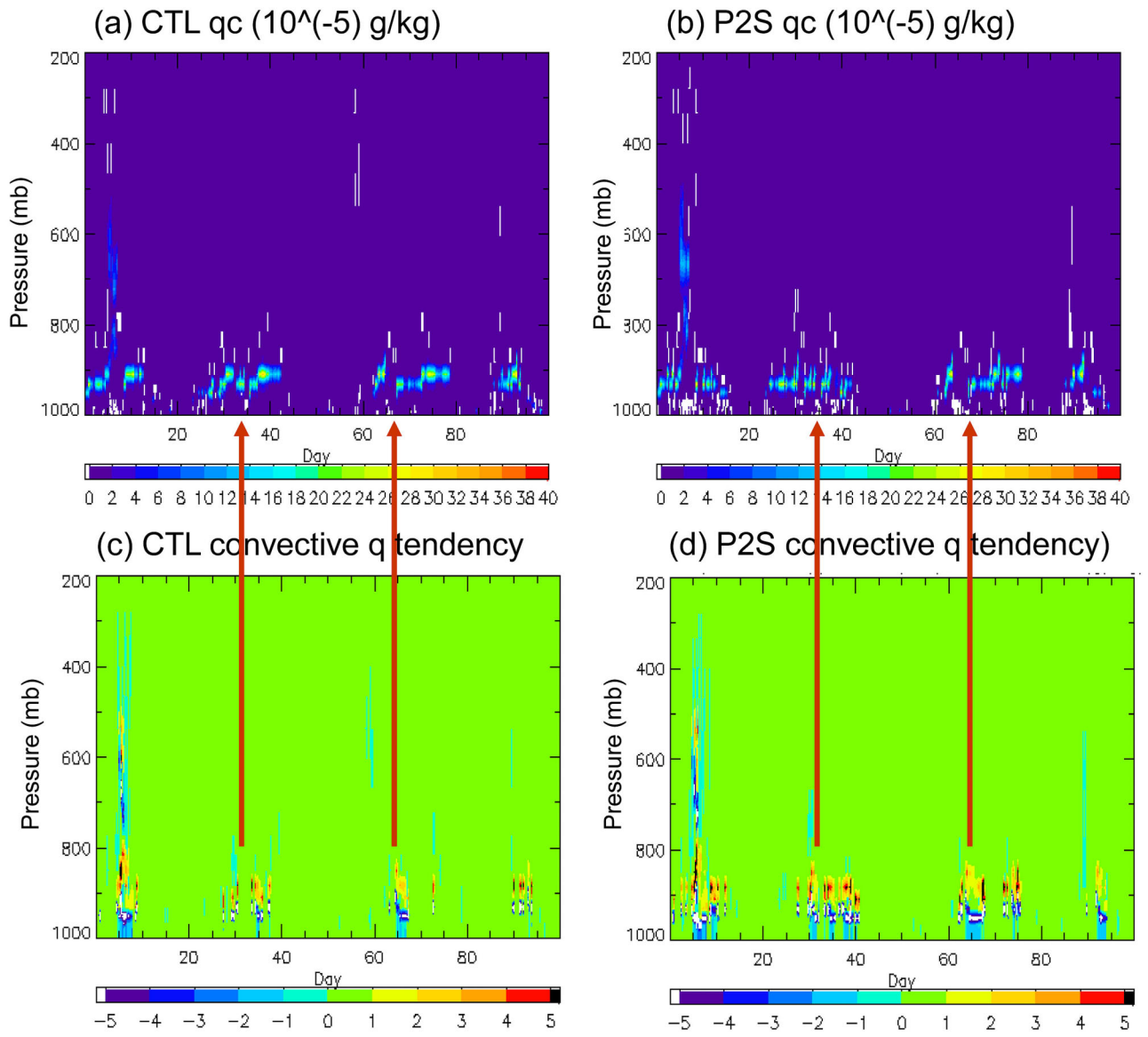

Figure 15. Time evolution of cloud liquid water in the GFDL model at S11 in (a) CTL, (b) P2S. Time evolution of the convective tendency of water vapor in (c) CTL, (d) P2S. The red vertical lines highlight the correspondence between the shallow convection and its impact on cloud water.

steady-state forcing produced cloud distribution and feedback along the GPCI similar to those in its GCM. In another example, we showed that the results from the CGILS steady forcing captured the background change of simulations from transient forcing, highlighting the robust cloud feedback mechanism in the model. We additionally showed with one model that the simulation from using the CGILS steady forcing offered independent insights to the role of different physical mechanisms in the model.

[37] The idealized design is a compromise between simplicity and realism. Although the correspondence with GCM behavior may not be perfect, it provides a useful framework to learn about the GCM cloud feedbacks under a common framework, to understand intermodel differences, and to foster and facilitate the analysis of GCM cloud feedbacks at the process level. This design also allows CRM and LES models to contribute to the cloud feedback studies. The current CGILS design is intended for the SST perturbed surrogate climate change and interpreting the GCM Cess experiments. Work is being planned to include additional change of increasing greenhouse gases in the perturbed climate, so that SCM results can be used to interpret cloud feedbacks in future climate changes in the models. The design and large-scale forcing data from this future work will be also posted at the CGILS website when it becomes available.

[38] **Acknowledgments.** Zhang's CGILS research is supported by the Biological and Environmental Research Division in the Office of Sciences of the US Department of Energy (DOE) through its FASTER project, and by the NASA Modeling and Analysis Program (MAP). Bretherton and Blossey acknowledge support from the NSF Center for

Multiscale Modeling and Prediction. Bony and Brient acknowledge support from the FP7-ENV-2009-1 European Project EUCLIPSE (244067).

References

Andrews, T., J. M. Gregory, M. J. Webb, and K. E. Taylor (2012), Forcing, feedbacks and climate sensitivity in CMIP5 coupled atmosphere-ocean climate models, *Geophys. Res. Lett.*, *39*, L09712, doi:10.1029/2012GL051607.

Bony, S., and J.-L. Dufresne (2005), Marine boundary layer clouds at the heart of cloud feedback uncertainties in climate models, *Geophys. Res. Lett.*, *32*, L20806, doi:10.1029/2005GL023851.

Bony, S., et al. (2006), How well do we understand climate change feedback processes? *J. Clim.*, *19*, 3445–3482, doi:10.1175/JCLI3819.1.

Brient, F., and S. Bony (2012), Interpretation of the positive low cloud feedback predicted by a climate model under global warming, *Clim. Dyn.*, doi:10.1007/s00382-011-1279-7.

Cess, R. D., et al. (1990), Intercomparison and interpretation of climate feedback processes in 19 atmospheric general circulation models, *J. Geophys. Res.*, *95*, 16,601–16,615, doi:10.1029/JD095iD10p16601.

Collins, W. D., et al. (2006), The Community Climate System Model Version 3 (CCSM3), *J. Clim.*, *19*, 2122–2143, doi:10.1175/JCLI3761.1.

Dee, D. P., et al. (2011), The Interim-ERA reanalysis: Configuration and performance of the data assimilation system, *Q. J. R. Meteorol. Soc.*, *137*, doi:10.1002/qj.828.

Donner, L. J., et al. (2011), The dynamical core, physical parameterizations, and basic simulation characteristics of the atmospheric component AM3 of the GFDL global coupled model CM3, *J. Clim.*, *24*, 3484–3519, doi:10.1175/2011JCLI3955.1.

GMAT (2004), The new GFDL global atmosphere and land model AM2–LM2: Evaluation with prescribed SST simulations, *J. Clim.*, *17*, 4641–4673, doi:10.1175/JCLI-3223.1.

Held, I. M., and M. J. Suarez (1994), A proposal for the intercomparison of the dynamical cores of atmospheric general circulation models, *Bull. Am. Meteorol. Soc.*, *75*, 1825–1830, doi:10.1175/1520-0477(1994)075<1825:APFTIO>2.0.CO;2.

Hourdin, F., et al. (2006), The LMDZ4 general circulation model: Climate performance and sensitivity to parametrized physics with emphasis on tropical convection, *Clim. Dyn.*, *27*(7–8), 787–813, doi:10.1007/s00382-006-0158-0.

Jablonowski, C., and D. L. Williamson (2006), Baroclinic wave test case for Dynamical cores of GCMs, *Q. J. R. Meteorol. Soc.*, *132*, 2943–2975, doi:10.1256/qj.06.12.

Khairoutdinov, M. F., and D. A. Randall (2001), A cloud resolving model as a cloud parameterization in the NCAR Community Climate System Model: Preliminary results, *Geophys. Res. Lett.*, *28*, 3617–3620, doi:10.1029/2001GL013552.

Medeiros, B., B. Stevens, I. Held, M. Zhao, D. Williamson, J. Olson, and C. Bretherton (2008), Aquaplanets, climate sensitivity, and low clouds, *J. Clim.*, *21*, 4974–4991, doi:10.1175/2008JCLI1995.1.

Mlawer, E. J., S. J. Taubman, P. D. Brown, M. J. Iacono, and S. A. Clough (1997), RRTM, a validated correlated-k model for the longwave, *J. Geophys. Res.*, *102*, 16,663–16,682., doi:10.1029/97JD00237.

Neale, R. B., and B. J. Hoskins (2000), A standard test for AGCMs including their physical parameterizations: I: The proposal, *Atmos. Sci. Lett.*, *1*, 101–107, doi:10.1006/asle.2000.0019.

Randall, D. A., and D. G. Cripe (1999), Alternative methods for specification of observed forcing in single-column models and cloud system models, *J. Geophys. Res.*, *104*(D20), 24,527–24,545., doi:10.1029/1999JD900765.

Randall, D. A. et al. (2007), Climate models and their evaluation, in *Climate Change 2007: The Scientific Basis. Contribution of Working Group I to the Fourth Assessment Report of the Intergovernmental Panel on Climate Change*, edited by S. Solomon et al., pp. 589–662, Cambridge Univ. Press, Cambridge, U. K.

Ringer, M. A., et al. (2006), Global mean cloud feedbacks in idealized climate change experiments, *Geophys. Res. Lett.*, *33*, L07718, doi:10.1029/2005GL025370.

Sato, S., et al. (2011), Improvements of top-of-atmosphere and surface irradiance computations with CALIPSO, CloudSat, and MODIS-derived cloud and aerosol properties, *J. Geophys. Res.*, *116*, D19209, doi:10.1029/2011JD016050.

Siebesma, A. P., et al. (2004), Cloud representation in general circulation models over the northern Pacific Ocean: A EUROCS intercomparison study, *Q. J. R. Meteorol. Soc.*, *130*, 3245–3267, doi:10.1256/qj.03.146.

Sobel, A. H., J. Nilsson, and L. M. Polvani (2001), The weak temperature gradient approximation and balanced tropical moisture waves, *J. Atmos. Sci.*, *58*, 3650–3665, doi:10.1175/1520-0469(2001)058<3650:TWTGAA>2.0.CO;2.

Stevens, B., et al. (2005), Evaluation of large-eddy simulations via observations of nocturnal marine stratocumulus, *Mon. Weather Rev.*, *133*, 1443–1462, doi:10.1175/MWR2930.1.

Teixeira, J., et al. (2011), Tropical and subtropical cloud transitions in weather and climate prediction models: The GCSS/WGNE Pacific Cross-Section Intercomparison (GPCI), *J. Clim.*, *24*, 5223–5256, doi:10.1175/2011JCLI3672.1.

Vecchi, G. A., et al. (2006), Weakening of tropical Pacific atmospheric circulation due to anthropogenic forcing, *Nature*, *441*, 73–76, doi:10.1038/nature04744.

Webb, M., et al. (2006), On the contribution of local feedback mechanisms to the range of climate sensitivity in two GCM ensembles, *Clim. Dyn.*, *27*, 17–38, doi:10.1007/s00382-006-0111-2.

Wyant, M. C., C. S. Bretherton, J. T. Bacmeister, J. T. Kiehl, I. M. Held, M. Zhao, S. A. Klein, and B. J. Soden (2006), A comparison of low-latitude cloud properties and their response to climate change in three AGCMs sorted into regimes using mid-tropospheric vertical velocity, *Clim. Dyn.*, *27*, 261–279, doi:10.1007/s00382-006-0138-4.

Wyant, M. C., C. S. Bretherton, and P. N. Blossey (2009), Understanding subtropical low cloud response to a warmer climate in a superparameterized climate model: Part I. Regime sorting and physical mechanisms, *J. Adv. Model. Earth Syst.*, *1*, 7., doi:10.3894/JAMES.2009.1.7

Xu, K.-M., A. Cheng, and M. Zhang (2010), Cloud-resolving simulation of low-cloud feedback to an increase in sea surface temperature, *J. Atmos. Sci.*, *67*, 730–748, doi:10.1175/2009JAS3239.1.

Zelinka, M. D., S. A. Klein, and D. L. Hartmann (2012), Computing and partitioning cloud feedbacks using cloud property histograms. Part I: Cloud radiative kernels, *J. Clim.*, *25*, 3715–3735, doi:10.1175/JCLI-D-11-00248.1.

Zhang, M., and C. S. Bretherton (2008), Mechanisms of low cloud climate feedback in idealized single-column simulations with the Community Atmospheric Model (CAM3), *J. Clim.*, *21*, 4859–4878, doi:10.1175/2008JCLI2237.1.

Zhang, M., and H. Song (2006), Evidence of deceleration of atmospheric vertical overturning circulation over the tropical Pacific, *Geophys. Res. Lett.*, *33*, L12701, doi:10.1029/2006GL025942.

Corresponding author: M. Zhang, School of Marine and Atmospheric Sciences, State University of New York at Stony Brook, Stony Brook, NY 11794-5000, USA. (minghua.zhang@stonybrook.edu)